Advanced Composite Materials
Publication details, including instructions for authors and subscription information:
http://www.tandfonline.com/loi/tacm20

Evaluation of the damage suppression effect of Ti-Ni shape memory alloy foils embedded in carbon fiber reinforced plastic laminates

Masataro Amano , Ichiro Taketa , Masakazu Kobayashi , Toshimichi Ogisu , Yoji Okabe & Nobuo Takeda

Version of record first published: 02 Apr 2012.

To cite this article: Masataro Amano , Ichiro Taketa , Masakazu Kobayashi , Toshimichi Ogisu , Yoji Okabe & Nobuo Takeda (2005): Evaluation of the damage suppression effect of Ti-Ni shape memory alloy foils embedded in carbon fiber reinforced plastic laminates, Advanced Composite Materials, 14:1, 43-61

To link to this article: http://dx.doi.org/10.1163/1568551053297076

Adv. Composite Mater., Vol. 14, No. 1, pp. 43–61 (2005)

Also available online - www.vsppub.com

Evaluation of the damage suppression effect of Ti-Ni shape memory alloy foils embedded in carbon fiber reinforced plastic laminates

MASATARO AMANO [1,*], ICHIRO TAKETA [1], MASAKAZU KOBAYASHI [1], TOSHIMICHI OGISU [2], YOJI OKABE [1] and NOBUO TAKEDA [1]

[1] *Takeda Laboratory, Department of Advanced Energy, Graduate School of Frontier Sciences, The University of Tokyo, 5-1-5, Kashiwanoha, Kashiwa-shi, Chiba, 277-8562, Japan*
[2] *Material Research Section, Research and Laboratory Department, Engineering and Development Center, Aerospace Company, Fuji Heavy Industries Ltd., 1-1-11, Yonan, Utsunomiya, Tochigi, 320-8564, Japan*

Received 8 April 2004; accepted 30 August 2004

Abstract—In this research, shape memory alloy (SMA) foils were embedded into carbon fiber reinforced plastic (CFRP) cross-ply laminates. When the tensile pre-strained SMA foil is heated, the SMA produces appropriate compressive stress (recovery stress) to suppress the transverse cracks in the laminates. In order to investigate the damage suppression effect, tensile loading–unloading tests were conducted for the CFRP cross-ply laminates. The test results implied that the recovery stress of embedded SMA foil suppressed the occurrence and the progress of the transverse crack. Then, to confirm that the damage suppression effect was caused by the embedded SMA foil, the one-dimensional (1D) shear-lag model considering the behavior of SMA was newly derived. Using this model, the progress of transverse crack density was predicted probabilistically. The simulation results showed the same tendency as the experimental results. As a result, it was proved that the embedment of SMA foils into CFRP laminates is effective to suppress the occurrence and growth of the transverse cracks.

Keywords: Shape memory alloys; CFRP; crack suppression; shear-lag model.

1. INTRODUCTION

Complicated microscopic damage, such as transverse cracks in off-axis plies, appear in laminates at much lower stress than the ultimate tensile strength. For much wider applications of advanced composites, including CFRP in various fields, it is

*To whom correspondence should be addressed. E-mail: masa@smart.k.u-tokyo.ac.jp

necessary to clarify the fracture mechanisms and then to fabricate smart composites that can suppress damage occurrence and progress in the laminates.

SMA has been expected to be one of the damage suppressing materials. Shimamoto *et al.* discussed Ti-Ni shape-memory fiber-reinforced epoxy matrix composite [1]. When the SMA is heated, it shrinks to its original length and generates compressive stress in the epoxy matrix. As a result, it was utilized to reduce K_1 of a side-notched TiNi/epoxy composite. In this research, SMA was improved to be used in the shape of foil in order to generate larger compressive stress. Moreover, the embedded SMA foil suppresses not only the progress but the occurrence of transverse cracks.

Many reports suggest that the embedment of the Ti-Ni SMA foil into a CFRP laminate is effective in suppressing the occurrence and progress of transverse cracks as shown in Fig. 1. Kobayashi *et al.* confirmed that pre-strained SMA provides a damage suppression effect in CFRP cross-ply laminates and the strength of the laminates increases by the embedment of SMA wires [2]. Ogisu *et al.* have been conducting studies on applications of CFRP laminates with embedded pre-strained SMA foil actuators [3]. They also reported that the prediction by shear-lag analysis for cross-ply CFRP laminates showed good agreement with the experimental data, which proved that the embedded SMA foil had the damage suppression effect [4].

In the previous paper [5], the authors suggested a newly developed constitutive model, called the extended Brinson model, to characterize the complicated behavior

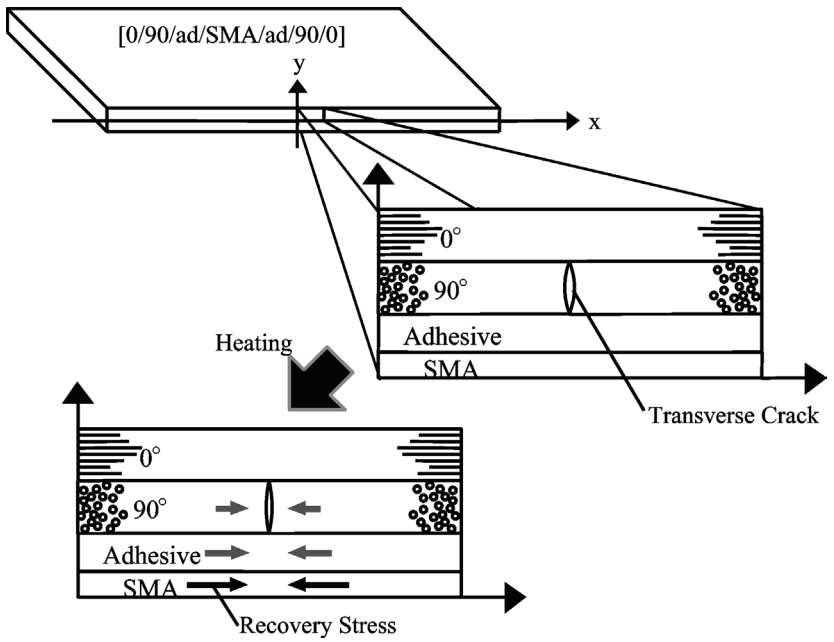

Figure 1. Mechanism of the recovery stress of an embedded SMA Foil to suppress the occurrence of transverse cracks in a CFRP cross-ply laminate.

of the Ti-Ni SMA foil accurately, which has a specific phase called R-phase. In this paper, the authors have tried to establish an analysis method to evaluate the damage suppression effect of the embedded Ti-Ni SMA foil with the extended Brinson model.

At first, tensile tests were carried out for CFRP cross-ply laminates with the embedded Ti-Ni SMA foil. The effect in the Ti-Ni SMA foil to suppress the increase in the transverse crack density in the laminates was examined. Then, the 1D shear-lag model with the extended Brinson model was newly developed. Using the new 1D shear-lag model, the relation between transverse crack density and the applied strain was calculated. Finally, through the comparison between these experimental and analytical results, we investigated whether the embedment of the Ti-Ni SMA foils into CFRP laminates is effective in suppressing the occurrence and growth of the transverse cracks.

2. EXPERIMENTS TO EVALUATE THE DAMAGE SUPPRESSION EFFECT OF Ti-Ni SMA FOIL

In order to evaluate the effect of Ti-Ni SMA foils in suppressing the occurrence and growth of transverse cracks in CFRP laminates, tensile loading–unloading tests were conducted at 25°C and 90°C on CFRP laminates in which SMA foils were embedded.

The Ti-Ni SMA foils used in these tests were Ti-50.2%Ni foils (Furukawa Electric Co. Ltd., thickness: 0.045 mm). For the improvement of the adhesion performance to resin, the surface of the foils was treated with 10% NaOH anode oxidation [6]. The CFRP laminates are T300/F593 (HEXCEL, prepreg thickness: 0.2 mm). Tables 1 and 2 show the mechanical properties of the CFRP and the SMA foil, respectively. All the symbols in Table 2 are described in Ref. [5]. Table 3 summarizes the three different types of laminates tested in this research. In these

Table 1.
Mechanical properties of the CFRP unidirectional laminates (T300/F593, Hexcel)

Mechanical properties		at 25°C	at 90°C
Elastic moduli (GPa)	E_1	112	109
	E_2	9.0	7.5
	G_{12}	4.55	4.0
Poisson's ratios	ν_{12}	0.34	
	ν_{23}	0.38	
Thermal expansion coefficients (/°C)	α_1	3.6×10^{-8}	
	α_2	2.7×10^{-5}	
Manufacturing temperature (°C)	T_0	180	

Table 2.
Mechanical properties of the SMA foil (Ti-50.2%Ni, Furukawa Electric Co. Ltd.)

Young's moduli (GPa)		Stress (MPa)		Strain (%)		Transition temperatures (°C)		Gradients (MPa/°C)	
E_{SAR}	23	σ_M^{band}	25	ε_L^M	5	M_s	3	C_M	5.1
E_{SIR}	23	σ_R^{max}	62	ε_L^R	0.6	R_s^*	49.7	C_R^*	18
E_M	26	σ_R^{min}	40			R_f^*	38.3	C_A	6
E_A	63	σ_A^{band}	20			A_s^*	47.9		

Table 3.
Configurations of the three types of laminates tested in this research

Specimens	Stacking configurations	
CF	[0/90]s	A CFRP cross-ply laminate with no SMA foil.
SMA0%	[0/90/ad/non pre-strained SMA/ad/90/0]	A CFRP cross-ply laminate with an SMA foil that was not pre-strained.
SMA4%	[0/90/ad/4% pre-strained SMA/ad/90/0]	A CFRP cross-ply laminate with an SMA foil whose pre-strain applied before the embedment was 4%.

configurations, 'ad' represents an epoxy adhesive film (Metlbond 1515-3, Cytec Industries, thickness: 0.127 mm) used for the increase in the adhesion between the CFRP laminate and the Ti-Ni SMA foil. The length and the width of the specimens are 150 mm and 15 mm, respectively.

All the tensile loading–unloading tests were carried out with Load Frame 5582 (Instron Corp.) at the tensile speed of 0.5 mm/min. The tests at 90°C were performed in a thermostatic chamber. Tensile strain was measured with a strain gage attached on the surface of the specimen, and the tensile load was measured with a load cell. After the laminate was unloaded, the positions and the numbers of transverse cracks in the 90° ply were observed with a high-resolution video microscope (Keyence, VH7000). This loading/unloading procedure was repeated until the specimen fractured completely.

Figure 2 shows the comparison of transverse crack density in 90° ply between the laminate without SMA foil and that with 4% pre-strained SMA foil at 25°C and 90°C. Also, Fig. 3 shows the comparison of transverse crack density in 90° ply between the laminate with non pre-strained SMA foil and that with 4% pre-strained SMA foil at 25°C and 90°C. The transverse crack density was defined as the average number of transverse cracks per centimeter, determined from the observation in the range of 3 cm with the video-microscope.

In Fig. 2a and Fig. 3a, the first crack strains of CF, SMA0% and SMA4% were found to be similar. Also, the tendency of the increase in the crack density is equal. These results reveal that the embedment of the Ti-Ni SMA foil does not deteriorate the mechanical properties of the laminates. Meanwhile, Fig. 2b shows that the first

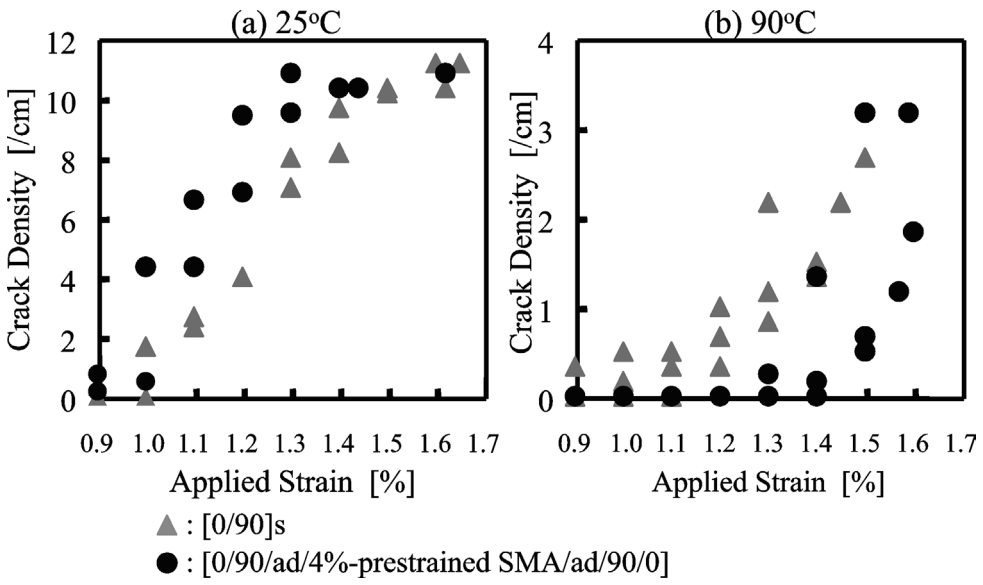

Figure 2. Comparison of transverse crack density in 90° ply between the laminate without SMA foil and that with 4% pre-strained SMA foil.

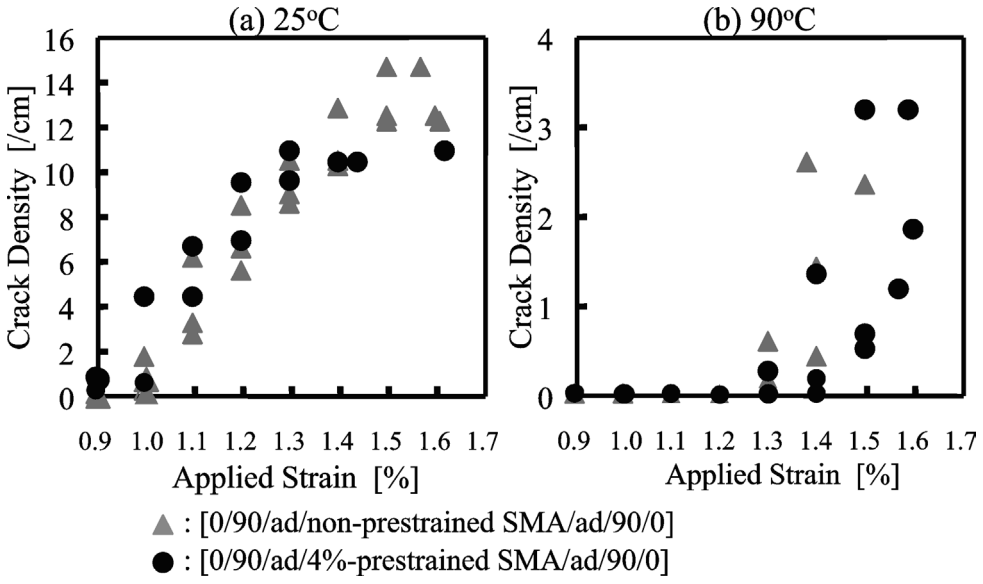

Figure 3. Comparison of transverse crack density in 90° ply between the laminate with non pre-strained SMA foil and that with 4% pre-strained SMA foil.

crack strain of SMA4% is about 0.4% larger than that of CF, and Fig. 3b shows that the first crack strain of SMA4% is 0.1% larger than that of SMA0% at 90°C. These results imply that the recovery stress of embedded Ti-Ni SMA foil suppresses the

occurrence of the transverse crack. The details of these experiments were described in our previous paper [7].

3. SIMULATION MODEL OF A CFRP CROSS-PLY LAMINATE WITH AN EMBEDDED SMA FOIL

In order to confirm that the damage suppression effect observed in the experiments was caused by the recovery stress of the 4% pre-strained Ti-Ni SMA foil embedded in CFRP, a theoretical analysis was conducted based on the extended Brinson model and a one-dimensional shear-lag model.

3.1. Extended Brinson model

As the authors proposed in the previous paper [5], the constitutive equation to represent the behavior of a Ti-Ni SMA is described as

$$\begin{aligned} \mathrm{d}\sigma = & \frac{1}{1+\varepsilon_L^R D\left(\xi^R,\xi^M\right)\dfrac{\partial \xi_S^R}{\partial \sigma}+\varepsilon_L^M D\left(\xi^R,\xi^M\right)\dfrac{\partial \xi_S^M}{\partial \sigma}} \\ & \times\left[D\left(\xi^R,\xi^M\right)\mathrm{d}\varepsilon-\left\{\varepsilon_L^R D\left(\xi^R,\xi^M\right)\frac{\partial \xi_S^R}{\partial T}+\varepsilon_L^M D\left(\xi^R,\xi^M\right)\frac{\partial \xi_S^M}{\partial T}\right.\right. \\ & \left.\left.+\alpha\left(\xi^R,\xi^M\right)D\left(\xi^R,\xi^M\right)\right\}\mathrm{d}T\right], \end{aligned} \tag{1}$$

where σ, ε and T are the tensile stress, Green strain and temperature respectively. ε_L is the maximum residual strain, and D and α represent the stiffness and thermal expansion coefficient tensors, respectively, which are functions of volume fractions ξ. The volume fraction ξ was divided into two parts, ξ_S and ξ_T, based on the micromechanics of an SMA material. ξ_S denotes a fraction of the stress-induced phase with a single martensitic variant and ξ_T represents a fraction of the purely temperature-induced phase with multiple variants. All superscripts represent the respective phases: M indicates martensitic phase and R indicates R-phase. These volume fractions ξ_S^M, ξ_S^R, ξ_T^M and ξ_T^R change according to the phase diagram in Fig. 4 and equation (1). As a result, the complicated behavior of the Ti-Ni SMA foil is analytically calculated.

3.2. 1D shear-lag model

In order to investigate the stress profile of the CFRP laminate with transverse cracks, a one-dimensional shear-lag model [8] is applied. Figure 5 is the schematic of the laminate configuration in the 1D shear-lag simulation. Interlaminar shear layers are assumed in both 0°-90° interface and SMA-90° interface. The 0° ply, the 90° ply and the SMA foil carry the normal stress σ. The shear layers carry only shear stress τ.

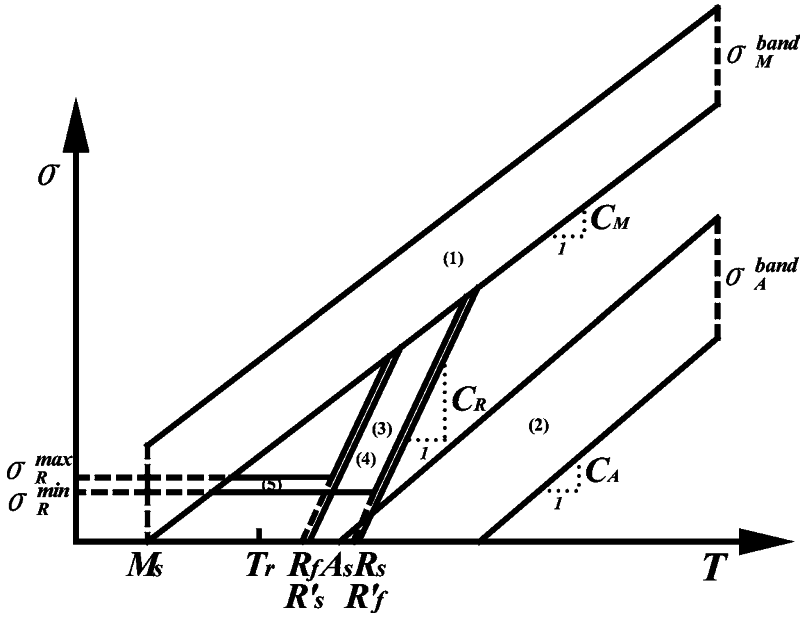

Figure 4. Critical stresses *versus* temperature representing transformations of Ti-Ni SMA. C_M and C_A are the slopes of the $\sigma_{crit}(T)$ curves for the austenitic phase to martensitic phase transformation and the reverse transformation, respectively. C_R is the slope of the $\sigma_{crit}(T)$ curves for austenitic phase to R-phase transformation and R-phase to austenitic phase transformation. *Tr* Room temperature, M_s martensite transformation start temperature, A_s reverse transformation start temperature, R_s R-phase transformation start temperature, R_f R-phase transformation finish temperature, R'_s R-phase inverse transformation start temperature, R'_f R-phase inverse transformation finish temperature.

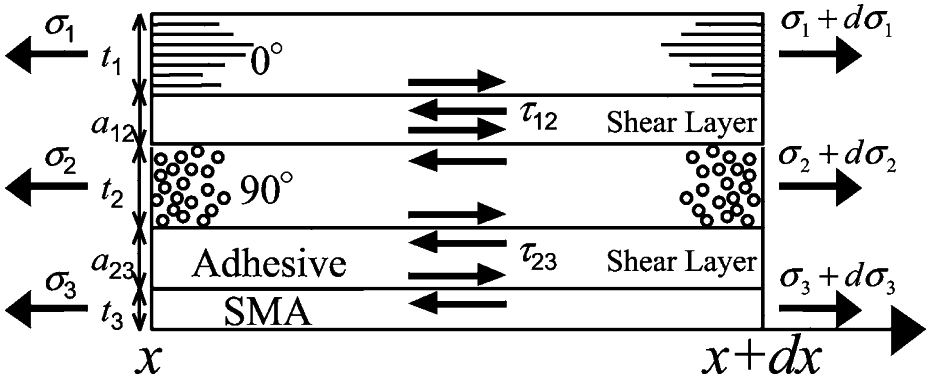

Figure 5. Schematic of the laminate configuration in 1D shear-lag simulation.

At first, the equilibrium of the tensile forces applied on each layer is represented as

$$t_1 \mathrm{d}\sigma_1 + \tau_{12}\mathrm{d}x = 0, \tag{2}$$

$$t_2 \mathrm{d}\sigma_2 + (\tau_{23} - \tau_{12})\mathrm{d}x = 0, \tag{3}$$

$$t_3 \mathrm{d}\sigma_3 - \tau_{23}\mathrm{d}x = 0, \tag{4}$$

where t denotes the thickness of the each layer. All the subscripts 1, 2 and 3 correspond to the 0° ply, the 90° ply and the SMA foil, respectively. Moreover, 12 and 23 correspond to the interlaminar shear layers in 0°-90° interface and SMA-90° interface, respectively.

By the substitution of the constitutive equations and compatibility equations into equations (2), (3) and (4), the equilibrium equations become

$$E_1 \frac{\mathrm{d}^2 u_1}{\mathrm{d}x^2} + \frac{G_{12}}{t_1}\frac{u_2 - u_1}{a_{12}} = 0, \tag{5}$$

$$E_2 \frac{\mathrm{d}^2 u_2}{\mathrm{d}x^2} + \frac{1}{t_2}\left(G_{23}\frac{u_3 - u_2}{a_{23}} - G_{12}\frac{u_2 - u_1}{a_{12}}\right) = 0, \tag{6}$$

$$E_3 \frac{\mathrm{d}^2 u_3}{\mathrm{d}x^2} - \frac{G_{23}}{t_3}\frac{u_3 - u_2}{a_{23}} = 0, \tag{7}$$

where a, u, E and G represent the thickness of the interlaminar shear layer, the displacement in the longitudinal direction, the Young's modulus of the each layer and shear modulus of the interlaminar shear layer, respectively.

While a_{23} is equal to the thickness of the adhesive, it is difficult to obtain the appropriate value of a_{12}, because it is a fitting parameter of the 1D shear-lag analysis. Thus, in this research, it was determined using 3D Finite Element Method. First, a tensile stress distribution was calculated with 3D FEM. Eight node iso-parametric solid elements were used. The dimensions of the model were as follows: 4 mm in the longitudinal direction, 15 mm in the width direction and 0.9 mm in the thickness direction. Details of the model were described in Fig. 6. These analyses

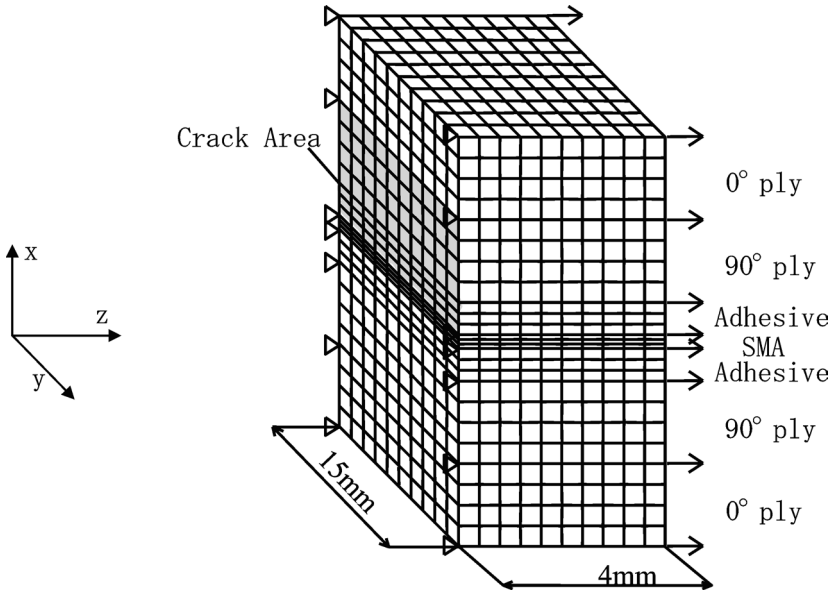

Figure 6. Schematic of 3D FEM model to determine the thickness of the interlaminar shear layer, a_{12}.

Table 4.
Thickness of the interlaminar shear layer a_{12} determined by the comparison of the calculation results between the 1D shear-lag model and the 3D FEM

Conditions	a_{12} (mm)
SMA0% 25°C	0.035
SMA0% 90°C	0.02
SMA4% 25°C	0.025
SMA4% 90°C	0.015

were conducted under the four types of conditions. Figure 7 shows the calculated longitudinal stress distributions in the 90° ply. As shown in Fig. 7, the thickness a_{12} was determined by fitting of the tensile stress distribution calculated by the 1D shear-lag model to that by the 3D FEM. Table 4 shows the value of a_{12} in four different conditions.

Then, by solving the differential equations (5), (6) and (7), the displacements of each layers u_1, u_2 and u_3 are determined as follows:

$$u_1 = C_1 e^{\xi_1 x} + C_2 e^{-\xi_1 x} + C_3 e^{\xi_2 x} + C_4 e^{-\xi_2 x} + C_5 x + C_6, \tag{8}$$

$$u_2 = P\left(C_1 e^{\xi_1 x} + C_2 e^{-\xi_1 x}\right) + Q\left(C_3 e^{\xi_2 x} + C_4 e^{-\xi_2 x}\right) + C_5 x + C_6, \tag{9}$$

$$u_3 = R\left(C_1 e^{\xi_1 x} + C_2 e^{-\xi_1 x}\right) + S\left(C_3 e^{\xi_2 x} + C_4 e^{-\xi_2 x}\right) + C_5 x + C_6, \tag{10}$$

where P, Q, R, S, ξ_1 and ξ_2 are described as

$$P = 1 - \frac{E_1 t_1 a_{12}}{G_{12}} \xi_1^2, \tag{11}$$

$$Q = 1 - \frac{E_1 t_1 a_{12}}{G_{12}} \xi_2^2, \tag{12}$$

$$R = \left(1 + \frac{a_{23} G_{12}}{a_{12} G_{23}} - \frac{E_2 t_2 a_{23}}{G_{23}} \xi_1^2\right)\left(1 - \frac{E_1 t_1 a_{12}}{G_{12}} \xi_1^2\right) - \frac{a_{23} G_{12}}{a_{12} G_{23}}, \tag{13}$$

$$S = \left(1 + \frac{a_{23} G_{12}}{a_{12} G_{23}} - \frac{E_2 t_2 a_{23}}{G_{23}} \xi_2^2\right)\left(1 - \frac{E_1 t_1 a_{12}}{G_{12}} \xi_2^2\right) - \frac{a_{23} G_{12}}{a_{12} G_{23}}, \tag{14}$$

$$\xi_1 = \sqrt{\frac{B + \sqrt{B^2 - 4AC}}{2C}}, \tag{15}$$

$$\xi_2 = \sqrt{\frac{B - \sqrt{B^2 - 4AC}}{2C}}, \tag{16}$$

where A, B and C are represented as follows:

$$A = t_1 E_1 + t_2 E_2 + t_3 E_3, \tag{17}$$

$$B = \frac{t_1 t_2 a_{12} E_1 E_2 G_{23} + t_2 t_3 a_{23} E_2 E_3 G_{12} + t_3 t_1 E_3 E_1 (a_{12} G_{23} + a_{23} G_{12})}{G_{12} G_{23}}, \tag{18}$$

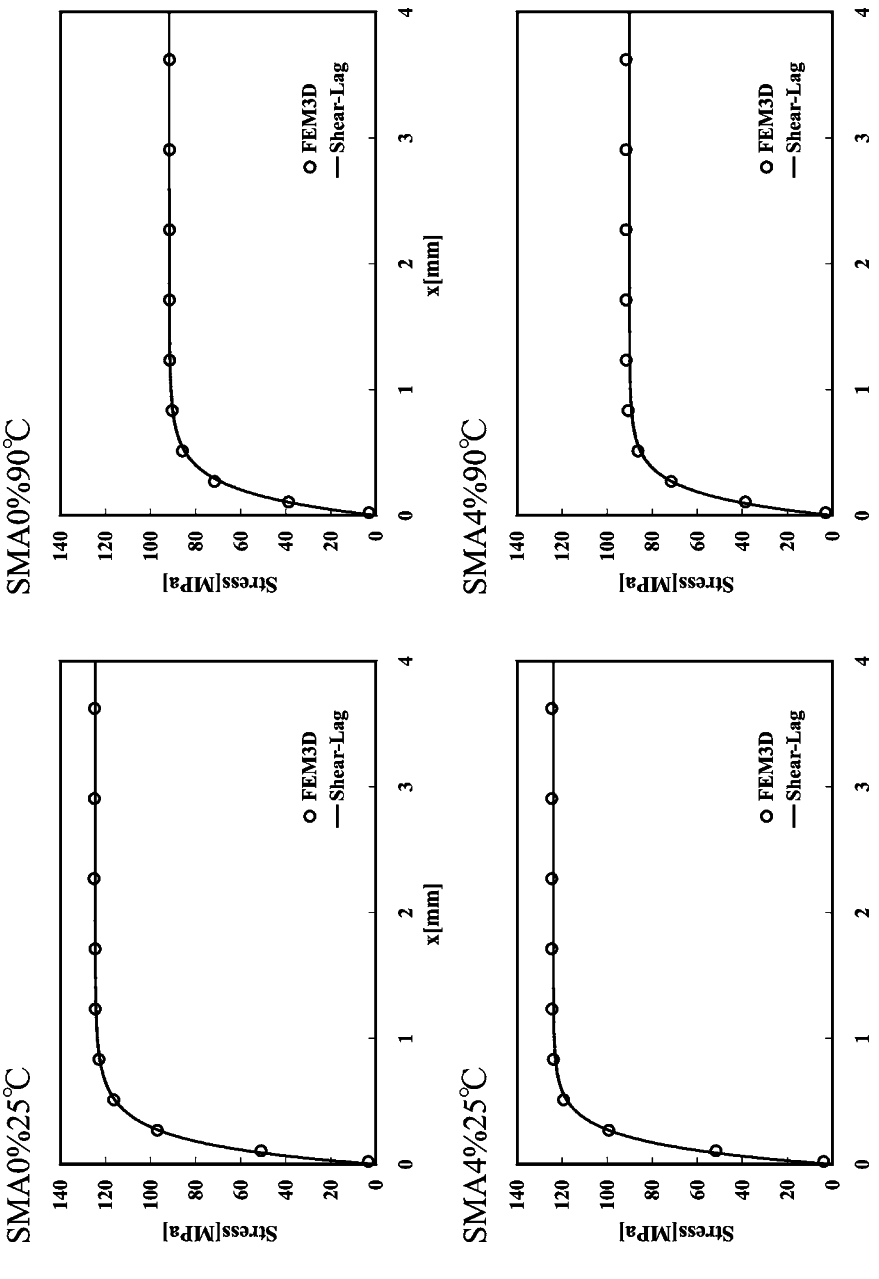

Figure 7. Comparison of the longitudinal stress distributions in the 90° ply between 1D shear-lag model and 3D FEM.

$$C = \frac{t_1 t_2 t_3 a_{12} a_{23} E_1 E_2 E_3}{G_{12} G_{23}}. \tag{19}$$

Using these constants, the tensile and shear strains ε_1, ε_2, ε_3, γ_{12} and γ_{23} are derived as

$$\varepsilon_1 = \xi_1\left(C_1 e^{\xi_1 x} + C_2 e^{-\xi_1 x}\right) + \xi_2\left(C_3 e^{\xi_2 x} + C_4 e^{-\xi_2 x}\right) + C_5, \tag{20}$$

$$\varepsilon_2 = P\xi_1\left(C_1 e^{\xi_1 x} + C_2 e^{-\xi_1 x}\right) + Q\xi_2\left(C_3 e^{\xi_2 x} + C_4 e^{-\xi_2 x}\right) + C_5, \tag{21}$$

$$\varepsilon_3 = R\xi_1\left(C_1 e^{\xi_1 x} + C_2 e^{-\xi_1 x}\right) + S\xi_2\left(C_3 e^{\xi_2 x} + C_4 e^{-\xi_2 x}\right) + C_5, \tag{22}$$

$$\gamma_{12} = \frac{P-1}{a_{12}}\left(C_1 e^{\xi_1 x} + C_2 e^{-\xi_1 x}\right) + \frac{Q-1}{a_{12}}\left(C_3 e^{\xi_2 x} + C_4 e^{-\xi_2 x}\right), \tag{23}$$

$$\gamma_{23} = \frac{R-P}{a_{23}}\left(C_1 e^{\xi_1 x} + C_2 e^{-\xi_1 x}\right) + \frac{S-Q}{a_{23}}\left(C_3 e^{\xi_2 x} + C_4 e^{-\xi_2 x}\right). \tag{24}$$

Moreover, the tensile and shear stresses σ_1, σ_2, σ_3, τ_{12} and τ_{23} are also derived as

$$\sigma_1 = E_1\left\{\xi_1\left(C_1 e^{\xi_1 x} + C_2 e^{-\xi_1 x}\right) + \xi_2\left(C_3 e^{\xi_2 x} + C_4 e^{-\xi_2 x}\right) + C_5 - \alpha_1 \Delta T\right\}, \tag{25}$$

$$\sigma_2 = E_2\left\{P\xi_1\left(C_1 e^{\xi_1 x} + C_2 e^{-\xi_1 x}\right) + Q\xi_2\left(C_3 e^{\xi_2 x} + C_4 e^{-\xi_2 x}\right) + C_5 - \alpha_2 \Delta T\right\}, \tag{26}$$

$$\sigma_3 = E_3\left\{R\xi_1\left(C_1 e^{\xi_1 x} + C_2 e^{-\xi_1 x}\right) + S\xi_2\left(C_3 e^{\xi_2 x} + C_4 e^{-\xi_2 x}\right) + C_5 - \alpha_3 \Delta T\right\}, \tag{27}$$

$$\tau_{12} = G_{12}\left\{\frac{P-1}{a_{12}}\left(C_1 e^{\xi_1 x} + C_2 e^{-\xi_1 x}\right) + \frac{Q-1}{a_{12}}\left(C_3 e^{\xi_2 x} + C_4 e^{-\xi_2 x}\right)\right\}, \tag{28}$$

$$\tau_{23} = G_{23}\left\{\frac{R-P}{a_{23}}\left(C_1 e^{\xi_1 x} + C_2 e^{-\xi_1 x}\right) + \frac{S-Q}{a_{23}}\left(C_3 e^{\xi_2 x} + C_4 e^{-\xi_2 x}\right)\right\}, \tag{29}$$

where ΔT represents the difference between the test temperature T_{test} and the cure temperature T_{cure}.

$$\Delta T = T_{\text{test}} - T_{\text{cure}}. \tag{30}$$

3.3. Boundary conditions

In this analysis, five boundary conditions were considered to represent a laminate with two transverse cracks at the interval of $2L$ in the 90° ply as shown in Fig. 8.

First, the tensile stress of the 90° ply is 0 on the crack surfaces.

$$1: \quad x = 0: \sigma_2 = 0, \tag{31}$$

$$2: \quad x = 2L: \sigma_2 = 0. \tag{32}$$

Then, the tensile strain of the 0° ply is equal to that of the SMA foil where a transverse crack exists:

$$3: \quad x = 0: \varepsilon_1 = \varepsilon_3, \tag{33}$$

$$4: \quad x = 2L: \varepsilon_1 = \varepsilon_3. \tag{34}$$

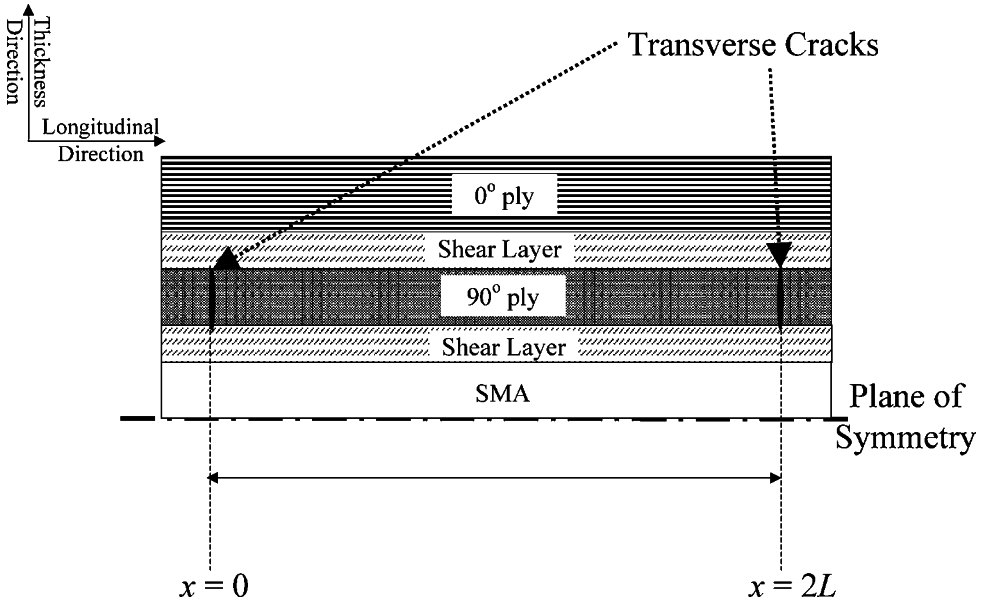

Figure 8. Schematic of the boundary conditions in the 1D shear-lag simulation.

Finally, in the middle of two cracks, the tensile strain in 0° ply is always equal to the applied strain measured with the strain gage

$$5: \qquad x = L: u_1 = L(\varepsilon_0 + \varepsilon^*), \tag{35}$$

where ε_0 is the applied strain measured with the strain gage and ε^* is the average thermal residual strain described as follows:

$$\varepsilon^* = \frac{t_1 E_1 \alpha_1 + t_2 E_2 \alpha_2 + t_3 E_3 \alpha_3}{t_1 E_1 + t_2 E_2 + t_3 E_3} \Delta T. \tag{36}$$

From these boundary conditions, the coefficients C_1, C_2, C_3, C_4 and C_5 are derived.

$$C_1 = \frac{U(S-1)}{\xi_1(1+e^{2\xi_1 L})}\left(\varepsilon_0 + \varepsilon_2^T\right), \tag{37}$$

$$C_2 = \frac{U(1-S)}{\xi_1(1+e^{2\xi_1 L})}\left(\varepsilon_0 + \varepsilon_2^T\right), \tag{38}$$

$$C_3 = \frac{U(1-R)}{\xi_2(1+e^{2\xi_2 L})}\left(\varepsilon_0 + \varepsilon_2^T\right), \tag{39}$$

$$C_4 = \frac{U(R-1)}{\xi_2(1+e^{2\xi_2 L})}\left(\varepsilon_0 + \varepsilon_2^T\right), \tag{40}$$

$$C_5 = \varepsilon_0 + \varepsilon^*, \tag{41}$$

where ε_2^T corresponds to the thermal residual strain in 90° layer and is shown as

$$\varepsilon_2^T = \frac{t_1 E_1(\alpha_1 - \alpha_2) + t_3 E_3(\alpha_3 - \alpha_2)}{t_1 E_1 + t_2 E_2 + t_3 E_3}\Delta T. \tag{42}$$

Moreover, C_6 becomes 0 since the displacements of all layers are 0 at $x = 0$.

3.4. Confirmation of the accuracy of the newly developed model

In order to confirm the accuracy of the 1D shear-lag model mentioned in the previous section, the stress profiles in the following four laminates were calculated. Each laminate configuration and condition are as follows:

SMA0%25°C: [0/90/ad/non pre-strained SMA/ad/90/0] at 25°C
SMA0%90°C: [0/90/ad/non pre-strained SMA/ad/90/0] at 90°C
SMA4%25°C: [0/90/ad/4% pre-strained SMA/ad/90/0] at 25°C
SMA4%90°C: [0/90/ad/4% pre-strained SMA/ad/90/0] at 90°C

The constitutive equation of SMA foil as shown in equation (1) should be introduced into this model to represent the recovery stress of the embedded SMA foil. Table 5 shows the dimensions and mechanical properties of the components of the laminate; elastic moduli and maximum compressive stress of the embedded SMA foil and thicknesses of layers.

Figure 9 shows the behavior of the SMA foil in the tensile loading–unloading test at 90°C. This behavior was calculated theoretically by the constitutive equation. As shown in this figure, the recovery stress of the SMA foil is nearly constant when the temperature is constant. Furthermore, since the equation (1) is an increment form, it is difficult to introduce the equation (1) directly into the 1D shear-lag model. Thus, the recovery stress was introduced into the thermal expansion coefficient of the SMA foil α_3 as follows.

Table 5.
Dimensions and mechanical properties of the components of the laminate; elastic moduli and maximum compressive stress of the embedded SMA foil and thicknesses of layers

Parameters	SMA0% 25°C	SMA0% 90°C	SMA4% 25°C	SMA4% 90°C
E_3 (GPa)	23.0	0.5	42.2	63.0
α_3 (/°C)	1.0×10^{-5}	1.0×10^{-5}	1.0×10^{-5}	1.0×10^{-5}
G_{12} (GPa)	1.34	0.55	1.34	0.55
G_{23} (GPa)	1.34	0.55	1.34	0.55
σ_r (MPa)	0	−124	0	−248
t_1 (mm)	0.18			
t_2 (mm)	0.18			
t_3 (mm)	0.02			
a_{23} (mm)	0.07			

t thickness of each layer, a thickness of adhesive.

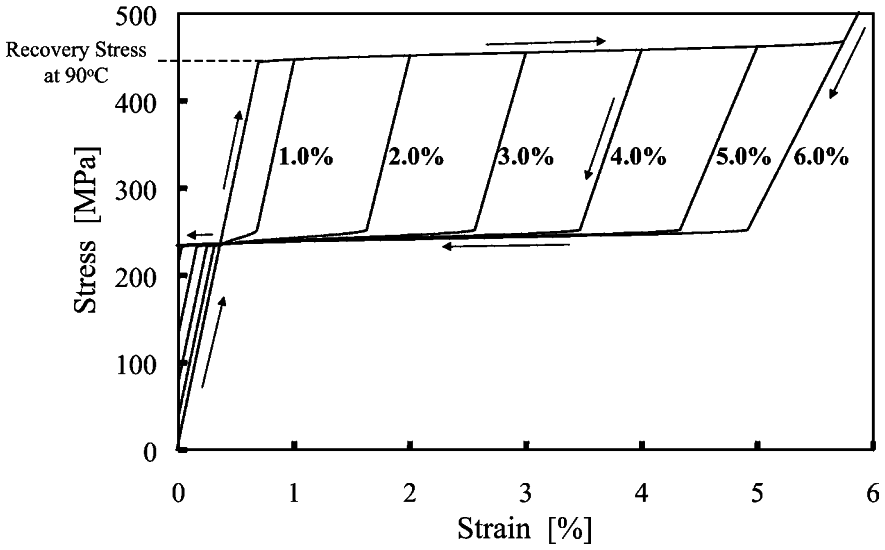

Figure 9. Behavior of the Ti-Ni SMA foil in the tensile loading–unloading test at 90 °C calculated by the constitutive equation.

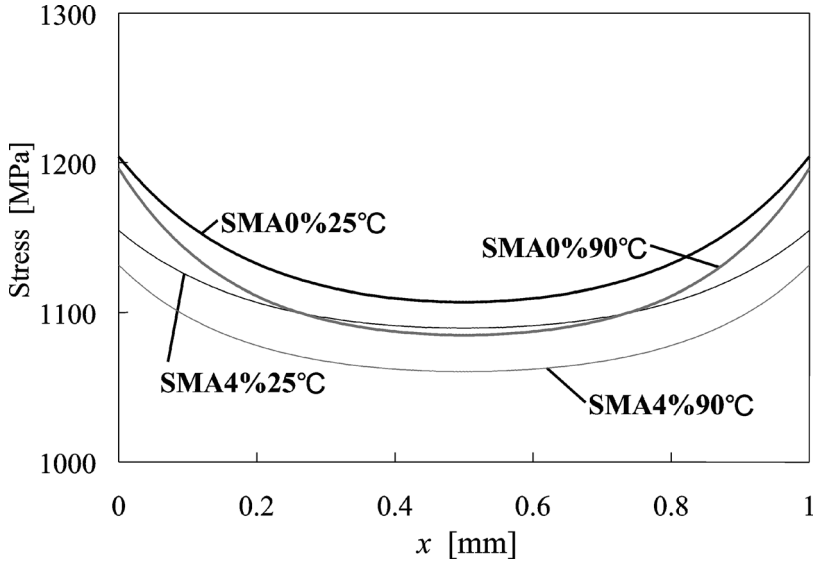

Figure 10. Longitudinal stress profiles in the 0° ply calculated by the 1D shear-lag model.

$$\alpha_3 = \alpha_{SMA} + \frac{\sigma_r}{\Delta T}, \tag{43}$$

where σ_r represents the recovery stress of the SMA foil at 90°C.

Figures 10, 11 and 12 show calculation results of the longitudinal stress profiles in 0° ply, 90° ply and SMA foil, respectively. These are the stress distributions between two transverse cracks at an interval of 1 mm, under tensile strain of 1%.

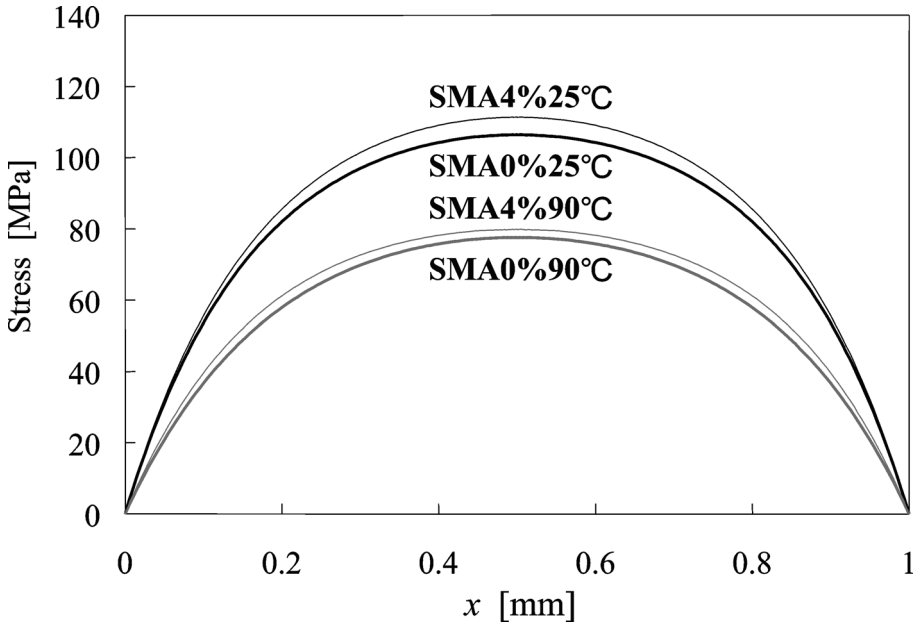

Figure 11. Longitudinal stress profiles in the 90° ply calculated by the 1D shear-lag model.

In Fig. 12, the tensile stress of SMA at 90°C is much larger than that at 25°C because of the recovery stress. Meanwhile, in Fig. 11, the tensile stress of the 90° layer at 90°C is smaller than that at 25°C. These results reveal that the tensile stress of the 90° layer in the laminate is relaxed by the recovery stress of the SMA foil at 90°C.

4. PREDICTION OF THE INCREASE IN THE TRANSVERSE CRACK DENSITY

In order to simulate the relation between the transverse crack density in 90° layer and the tensile strain ε_0 applied to the laminate, a probabilistic Monte Carlo simulation was carried out as follows.

4.1. Initiation of transverse cracks in the 90° layer

The probability of fracture strength in the 90° ply is assumed to obey a two-parameter Weibull distribution [8]. The probability distribution function is

$$F(\sigma) = 1 - \exp\left\{-\frac{V}{V_0}\left(\frac{\sigma}{\alpha}\right)^{\beta}\right\}, \tag{44}$$

where β is a shape parameter, α is an average fracture strength that corresponds to a scale parameter and V_0 is a standard volume. In order to determine the α and β, the tensile tests were performed for the 90° unidirectional laminate. The number of specimens was approximately 20 for each temperature. Table 6 shows the Weibull

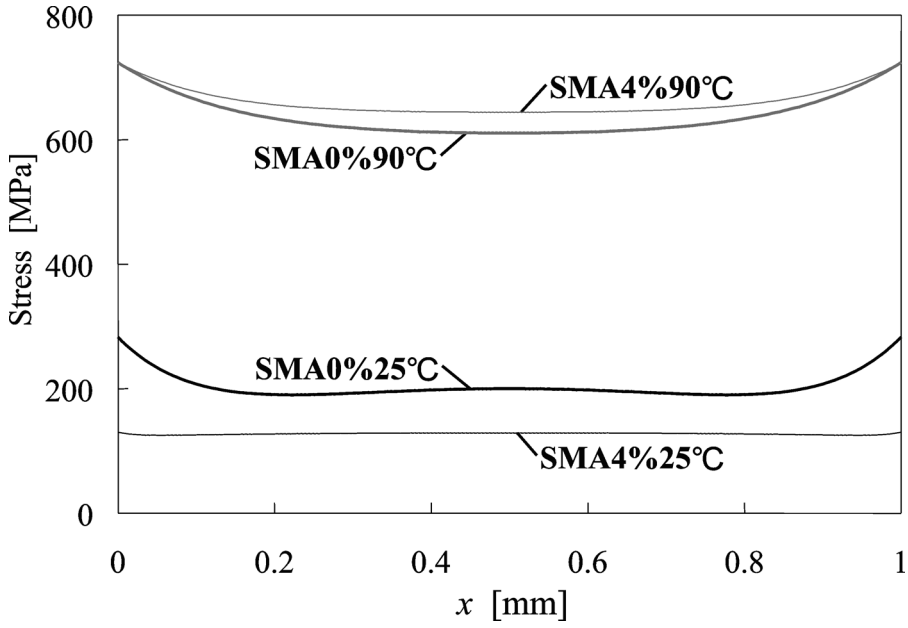

Figure 12. Longitudinal stress profiles in the SMA foil calculated by the 1D shear-lag model.

Table 6.
Parameters of the Weibull distribution at RT and 90°C obtained by Weibull plotting

	α	β
RT	77.3	8.8 ($n = 19$)
90°C	69.4	18.9 ($n = 20$)

parameters of the tensile strength distributions of the 90° ply unidirectional laminate at RT (room temperature, 25°C) and 90°C.

4.2. Probabilistic prediction of transverse crack density

The 90° ply in the laminate was assumed to be divided into small elements. The length of each element was determined as follows. First, the number of transverse cracks just before the final fracture was counted in the experiment. Then, the number of the elements in the 1D shear-lag model was determined to be equal to the measured number of the cracks in order to adjust the final crack density in the calculation to that in the experiment. According to this procedure, the length of each element was determined to be 0.75 mm. Using this length, the volume V of each element in the equation (44) was obtained. The crack interval $2L$ was also determined from the measured crack density at each strain level. Rewriting the equation (44), we can determine the fracture strength in 90° layer σ_c at each element as

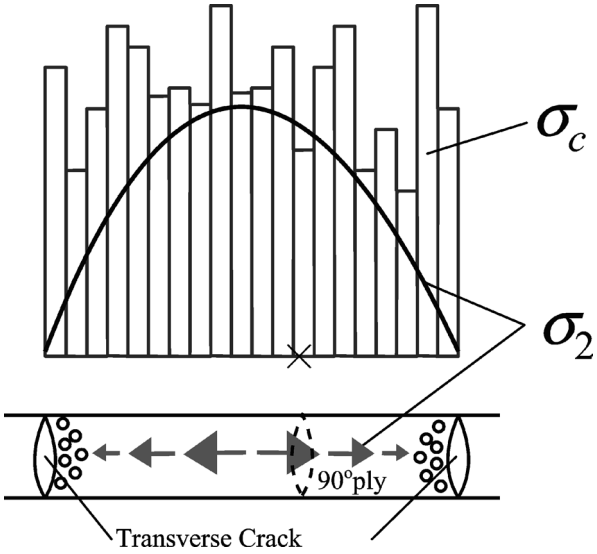

Figure 13. Procedure of the simulation to predict the occurrence of a new transverse crack.

$$\sigma_c = \alpha\left(\frac{V_0}{V}\ln\frac{1}{1-F}\right)^{1/\beta}, \tag{45}$$

where the probability distribution F at each element follows the Weibull theory. Before the calculation, the fracture strength of each element was determined from the equation (45).

Then, stress distribution in the 90° layer σ_2 is calculated by the 1D shear-lag model constructed in the previous section. When the tensile stress in an element is larger than its fracture strength, the element fails as shown in Fig. 13. Through the repetition of this process, the increase in the transverse crack density can be calculated.

In this model, the constraint effect was taken into account [8] by replacing ε_0 by $\varepsilon_0 + \varepsilon_r$, where ε_r is called the constraint strain, which is the difference between the first cracking strain predicted by the energy criterion and that predicted by the strength criterion.

Figure 14 shows the comparison of the increase in the transverse crack density between the predictions by this model and the experimental results at the temperatures of 25 °C and 90 °C. Three calculation results are plotted simultaneously at each temperature. This figure shows that the simulation well reproduces the experimental result. As a result, it was found that the embedment of the SMA foil into CFRP laminate was effective in suppressing the occurrence and progress of transverse cracks.

5. CONCLUSIONS

In this research, loading–unloading tests were performed for CFRP cross-ply laminates in different laminate configurations. The first crack strain of the specimens

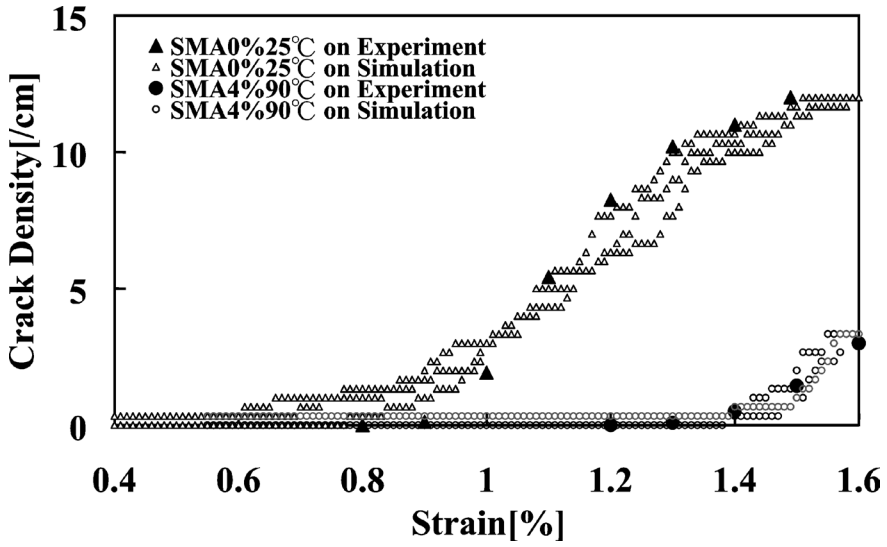

Figure 14. Comparison of the increase in transverse crack density between experiment and simulation.

with 4% pre-strained SMA foils was larger than those with 0% pre-strained SMA foils. These results indicated that the recovery stress of SMA potentially had a damage suppression effect.

Then, the 1D shear-lag model of the damaged laminates with embedded SMA foils was newly suggested. The constitutive equation of Ti-Ni SMA was taken into account in the model. From this model, it was found that the tensile stress of the 90° layer in the laminate was relaxed by heating of the laminate up to 90°C.

Moreover, the increase in the transverse crack density was predicted by a Monte Carlo Simulation. By comparison between the measured and calculated transverse crack densities, the embedment of pre-strained SMA foil in CFRP cross-ply laminate was confirmed to be effective in suppressing the occurrence and growth of the transverse cracks.

REFERENCES

1. A. Shimamoto, J. S. Hawong and H. J. Lee, Development of shape memory Ti-Ni fiber reinforced epoxy matrix composite and its properties, *J. Eng. Mat. and Tech.* **124** (4), 390–396 (2002).
2. A. Kobayashi, S. Ogihara, H. Yoshinari and N. Takeda, Damage development in composite laminates with embedded SMA wires, in: *Proc. 6th Japan International SAMPE Symposium*, pp. 65–68 (1999).
3. T. Ogisu, M. Nomura, H. Kikukawa and N. Takeda, Development of health monitoring system using embedded SMA foils in CFRP laminates, in: *Proc. 2nd International Workshop on Structural Health Monitoring*, F.-K. Chang (Ed.), pp. 317–326 (1999).
4. T. Ogisu, M. Nomura, N. Ando, J. Takaki, D.Y. Song and N. Takeda, Development of damage suppression system using embedded SMA foil in CFRP laminates, in: *Proc. SPIE*, Vol. 4333, pp. 387–398 (2001).

5. I. Taketa, M. Amano, M. Kobayashi, T. Ogisu, Y. Okabe and N. Takeda, Modeling of thermo-mechanical behavior of Ti-Ni shape memory alloy foils embedded in carbon fiber reinforced plastic laminates, *Adv. Composite Mater.* **14**, 25–41 (2005).
6. T. Ogisu, N. Ando, J. Takaki, T. Okabe and N. Takeda, Improved surface treatment of SMA foils and damage suppression of SMA-foil embedded CFRP laminates, *J. Intel. Mater. Syst. Struct.* **12** (4), 265–270 (2001).
7. I. Taketa, M. Amano, Y. Okabe and N. Takeda, Damage detection and suppression system of CFRP laminates with FBG sensor and SMA actuator, *Trans. MRS-J* **28**, 675–678 (2003).
8. N. Takeda and S. Ogihara, *In situ* observation and probabilistic prediction of microscopic failure processes in CFRP cross-ply laminates, *Compos. Sci. Technol.* **52**, 185–195 (1994).